POLITECNICO DI MILANO

SCHOOL OF INDUSTRIAL AND INFORMATION ENGINEERING

MASTER OF SCIENCE IN AUTOMATION AND CONTROL ENGINEERING

Human arm impedance estimation for hands-on control: a comparison between two approaches

Supervisor: Prof. Luca BASCETTA

Master Graduation Thesis by:
Gabriele LAINI
920661

Academic Year 2019-2020

Alla mia famiglia

Ringraziamenti

Ringrazio i miei genitori per il sostegno e per avermi appoggiato nelle mie scelte, nella speranza di essere riuscito a renderli fieri di me.
Ringrazio mia sorella Lucia, per essere sempre stata al mio fianco.
Ringrazio una persona per me molto speciale, Marta, per essere sempre stata al mio fianco nel momento del bisogno.
Ringrazio i miei colleghi universitari, Daniele, Lorenzo, Luca e Matteo, per avermi accompagnato in questi anni di studio.
Ringrazio i miei amici Erika, Mattia, Sophia, per essermi stati vicini e per avermi aiutato a staccare dalla monotonia universitaria.
Ringrazio Fabio che è sempre stato gentile e disponibile nel fornirmi il materiale per poter completare i miei studi.
In ultimo, ringrazio il mio relatore, Professore Luca Bascetta, per la sua disponibilità durante il percorso di tesi.

Contents

List of Figures

List of Tables

Abstract

An ever greater need of automation in factories, togheter with an ever changing market, have led the modern robotics industry to an evolution in which the collaborative robots are rising significantly. Consequently, the physical human-robot interaction is becoming more and more frequent, and it is important to use a control that guarantees an always stable system and an easy collaboration. To enable this, the impedance control, which is widely used in collaborative operations, comes in handy. However, this type of control needs to estimate the impedance parameters of the operator arm, so as to act in the best possible way understanding the intentions of the human operator, and adapt its parameters to act accordingly.

This work proposes a method for the estimation of the impedance parameters of the operator arm during the collaborative operations, which is minimally invasive and can be used in real time. It is based on the EMG signals coming from the main muscles of the human arm and on the data of the operator posture.

First, the kinematic and the dynamic model of the operator arm are built, using the same method used for the robotic manipulators; later a methodology for obtaining the parameters for these models, from sensors placed on the human arm, is presented. Then, the criteria for the identification of the parameters of the impedance model, and the experimental procedure to extract the necessary data to calculate them, are reported. Lastly the method proposed in this work has been compared with a previous one.

Key words: Human-robot interaction, human arm impedance, human modelling, impedance control.

Sommario

Un sempre maggiore bisogno di automatizzazione nelle aziende, unito ad un mercato in continuo cambiamento, hanno portato l'industria robotica moderna ad un'evoluzione in cui i robot collaborativi stanno aumentando in modo significativo. Di conseguenza, l'interazione fisica tra uomo e robot sta diventando sempre più frequente, per cui è importante utilizzare un controllo che garantisca di avere sempre un sistema stabile e una facile collaborazione. Per consentire ciò, ci viene in contro il controllo di impedenza che è largamente usato in operazioni collaborative; questo controllo però, per intervenire al meglio, necessita di conoscere i parametri di impedenza del braccio dell'operatore, in modo da poter intuire le intenzioni di quest'ultimo e adattare i propri parametri per agire di conseguenza.
Questo lavoro propone un metodo per la stima dei parametri d'impedenza del braccio dell'operatore, durante le operazioni collaborative, poco invasivo e da poter utilizzare in tempo reale; esso si basa sui segnali EMG provenienti dai principali muscoli del braccio e dai dati sulla postura di quest'ultimo.
Come prima cosa, viene costruito il modello cinematico e dinamico del braccio dell'operatore, utilizzando la stessa metodologia impiegata per i manipolatori robotici; successivamente è presentata una procedura per ottenere i parametri per questi modelli attraverso dei sensori posizionati sul braccio umano. In seguito, verranno riportati: il criterio per l'ottenimento di tutti i parametri del modello d'impedenza, e la procedura sperimentale con cui estrarre i dati necessari per calcolarli. In ultimo, il metodo descritto in questo lavoro viene confrontato con uno utilizzato in precedenza.

Parole chiave: Interazione uomo-robot, impedenza del braccio umano, modellistica umana, controllo ad impedenza.

Introduction

From the second half of the 20th century, the robots have becoming a fundamental part of factory production, they are especially used in repetitive and dangerous operations. However, some tasks can be either too complex or too expensive to automate, and either too difficult or too heavy to make them manually, in these cases the human-robot collaboration becomes necessary; and this is why the use of collaborative robots are becoming more and more popular. With the growth of the collaborative robots market, the need for a safe control of human-robot interaction has grown up too; the most used control to fulfil this request is the impedance control. In the collaborative operations, where the impedance control is applied, the operator is able to manipulate directly the robot by applying forces and torques to the robot end-effector, nevertheless to guarantee a stable interaction the controls parameters, in particular the damping or the stiffness, are set to high values but in this way the robot becomes more difficult to move for the operator. This choice, of the controls parameters, is done because the operator have the ability to vary its arm endpoint impedance depending on what he wants to do; so the controller, that not know the operator intention, has to mantain the collaboration stable in any case. The online adaptation of the impedance parameters according to the impedance of the operator's arm has been proposed in literature to improve the cooperation; in particular this impedance estimation has been done through the EMG signals coming from the principal muscles of the upper arm (biceps and triceps).

In this scenario, the aim of this thesis is to present an online, non-invasive, computationally efficent, and EMG based human arm impedance estimation method. First, the reduced complexity model is presented; then the human arm triangle model is described as an intuitive and simple tool to describe the arm posture and the corresponding joints angle and endpoint stiffness profile from the sensors data. At the same time, the experimental procedures to obtain data to build the method are described, and in particular from these experiments are obtained the experimental: inertia term, dumping term, and stiffness term. The first term obtained is used as constant in the model, the second one is used to discretize the dumping trajectory, and the last term is used to calculate the minimum activation joint stiffness matrix and a co-activation index, defined based on the EMG signals, that rescales this matrix; both used in the stiffness model. Finally, the estimation method is simulated, starting from the design of the kinematic and dynamic model of the human arm built in the same way as for robotic manipulators; then the impedance model parameters are derived from experimental data, and the obtained impedance profile is compared with another coming from an estimation method previously used.

All the impedance parameters are taken into account to realize a complete impedance estimation model of the human arm.

Thesis organization

The thesis is organized as follow:

- **Chapter 1**: A brief introduction on the collaborative robots focusing on their benefit and their footprint on the robotics market.
- **Chapter 2**: In this chapter the human-robot interaction is described in the first section, and in the second one a brief explanation of the impedance control is done. The third section explains the robot dynamic model; in the last one the impedance control is applied to a manipulator.
- **Chapter 3**: The human arm dynamic model is first described, followed by an impedance model for the arm. Later, all the techniques, the tools, and the experimental procedures to obtain the data to build the impedance model are described.
- **Chapter 4**: All the simulations needed to obtain, from data, all the necessary parameters for the human arm endpoint stiffness model are reported, with the simulation results. Finally, a brief comparison with a previously used method is done.

Chapter 1

Collaborative Robots

1.1 Industrial Robotics in the 20th Century:

Industrial robots born from the idea to build devices that could substitute humans in repetitive or heavy tasks. The evolution of industrial robots can be subdivided in four generations that span from ‘50s to the present day.

The first industrial robot generation rise at the beginning of ‘50s up to the end of ‘60s. The robots of this generation were provided with low-tech equipment and with a basic control; they are only programmable machine with no control on task execution. Movement of the axes were managed by mechanical stops that limit movement of the axes, also this kind of robots are actuated by hydraulic actuator “controlled” via relays which switched solenoid valves.

Figure 1.1: Example of robot of first generation (the Unimate robot).

The second generation of industrial robots spans from the end of ‘60s to the end of ‘70s. These robots could carry out more complex tasks with respect to the ones of the earlier generation since they could recognize the external enviroment, even if only in a basic way. They were controlled by microprocessor or PLC and could be programmed by an operator using a teach box.
These kind of robots were equipped with servo-controllers which enable them to perform point-to-point motion and continues path, however they had a limited versatility since they were designed for a specific task. This generation of robot saw the transition from hydraulic to electric actuators, thanks to the wide diffusion of the microprocessors. These technology changes increased productivity and reduced the cost.

Figure 1.2: Example of robot of second generation (The Stanford Arm).

The third generation starts at the end of ‘70s to the end of the century. This generation of industrial robots could be used to perform a large amount of different tasks since they could be programmed either on-line or off-line by a PC. This ease of programming in addition at the implementation of advanced sensors on board (e.g. force sensors, laser scanners, cameras) made possible the interaction with environment and humans, in order to carry out more complex tasks.

Figure 1.3: Example of robots of the third generation (AdeptOne SCARA robots)

At the beginning of the 21st century the fourth generation of industrial robots starts, and is still continuing. Robots of this generation have a huge computational power that make them able to perform complex control strategies, deep learning, logical reasoning, collaborative behaviour.

1.2 Collaborative Robotics:

The collaborative robots, or cobots, are all the robots designed to work alongside humans with shared spaces or in close proximity, when used in industry they are called collaborative industrial robots.
The International Federation of Robotics divide collaborative robots in two groups, this division is based on whether or not the ISO 10218-1:2011 norm is fulfilled. This norm “specifies requirements and guidelines for the inherent safe design, protective measures and information for use of industrial robots” [1].

In the first group we have the robots designed for a human robot interaction, but they do not fulfil the aforementioned norm. These robots are however considered safe since they

follow different safety standards. An example of cobots belonging to this group are the home cleaning robots that follow the in-house safety standards.

The second group contain industrial robots that fulfil the ISO 10218-1:2011 norm. This norm allows four type of different collaborative operations (Figure 1.4).

The first collaborative operation is safety-rated motion stop, where the industrial robots work in a separate workspace, normally surrounded by a cage, with respect to workers; but they can enter at any time in this space. If the cage is opened or the worker enters inside the collaborative workspace the robot become standstill without an interruption of the power, in this way the robot is ready to resume as soon as the worker leaves the collaborative workspace.

The next operation is hand guiding, where the robot motion happens only through direct input of the worker. This input is given by moving manually the robot end effector that is equipped with a force/torque sensor, used to detect operator intention.

The third collaborative operation admitted is the speed and separation motoring. This operation is a kind of evolution of the first one, indeed robot can behave in three different ways depending on the distances between the worker and the robot. The robot works normally until the distance from worker becomes less then a threshold, then robot speed is reduced and if the distance is further reduced below a second threshold the robot speed is reduced again and so on until the distance is below the minimum threshold. In this last case the robot standstill without an interruption of the power as long as the distance exceeds the narrow threshold.
The distance between the robot and the worker is measured by sensors installed inside the collaborative workspace.

The last collaborative operation admitted from the norm is power and force limiting by inherent design or control, the robots used in this scenario are equipped with force and speed sensor at joints to measure the entities of the contact with the operator, that has not to exceed some limits.

In the second and the fourth cases, where the robot works a direct contact with worker, the robots are built with some technical solutions to not injure worker following a collision. These solutions include rounded contours, lightweight materials, etc.

Figure 1.4: Type of collaborative operation admitted by ISO 10218-1

1.2.1 Benefits of collaborative robotics

The cobots, with respect to standard robots, give some advantages. The first one is the short installation, which require few time because cobots are light, compact, programmed by a user friendly software and mobile applications, without too specific knowledge. Also, they are able to remember actions that are taught to them manually. This benefit makes them flexible, so they can change task easily.
Besides cobots do not need physical barriers, this enables them to be used in the same workspace with humans in a safety manner, and reducing the floor occupation. For this reason, they are employed in collaboration to workers to share advantages of both, like: precision, strength, repeatability of the robot, combined with adaptability and intelligence of the worker. They are also used to help worker with heavy and boring tasks as for example move or keep in position heavy object.

1.2.2 Collaborative robotics market

In the last few years collaborative robot are becoming more and more common in industry thanks to the continuous innovation in this branch, and is expected to be a breakthrough in the coming years. Indeed the “collaborative robot market is projected to grow from USD 981 million in 2020 to USD 7,972 million by 2026” [2]. In particular in this forecast cobots with payload less than 5 kg will take the larger part of this market, since they are cheap and need less space compared with the cobots with bigger payload; consequently they are the best choice for the companies that want to start to become automate. The sector that will be most affected by light payload robots is the electronic one, where the cobots will be use alongside worker to help them to handle and assemble fragile circuit boards.

A big boost for this market will be given by programming software, since cobots producers are investing on the development of more and more intuitive programming software as well as application specific ones. This development will bring cobots to be increasingly easy and fast to deploy for new users.

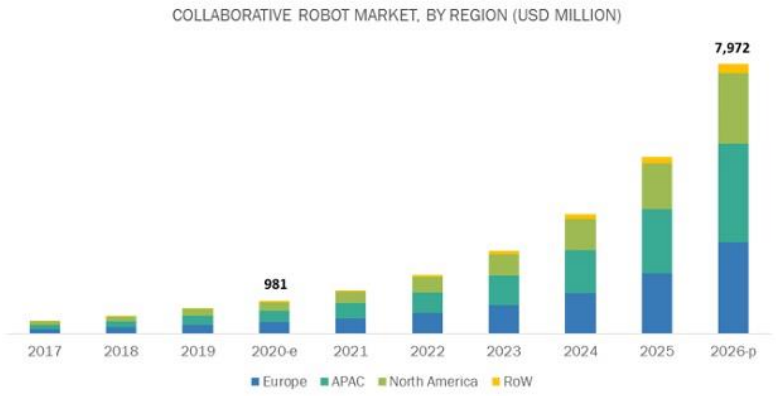

Figure 1.5: Collaborative robot market, by region (USD million)

Chapter 2

Impedance control

2.1 Robot interaction control

In a large part of the industrial robot applications, the robot is assumed to be in a free environment where the dynamical interaction with objects can be either absent or negligible. In these cases, the robot is considered as a stand-alone system, and the traditional control strategies are sufficent for a correct execution of the tasks. However, there are operations which require that the robot has to interact either with the environment, or with other devices, or with humans; in these scenarios the assumption of a free environment is not true anymore and a traditional industrial robot, as it is, is not able to perform these tasks. In order to allows a robot interaction with the environment, the robot needs external sensors (such as force/torque sensors, vision sensors, etc.) that make the robot aware of what happens around it, and a control strategy able to manages these new signals coming from these sensors to get the wanted behaviour.

2.1.1 Force/torque sensors

The force/torque sensors are used in all the application where the control of the interaction force is needed. These sensors are usually placed in the manipulator wrist near the working tool in a way as to return the three component of the interaction force and the three components of the moment with respect to a local frame. The sensing part of these sensors is based on strain gauges made with piezoelectric material that changes its electrical resistance consequently to a strain; by measuring the voltage at the ends of the sensing part is possible to obtain the strain.

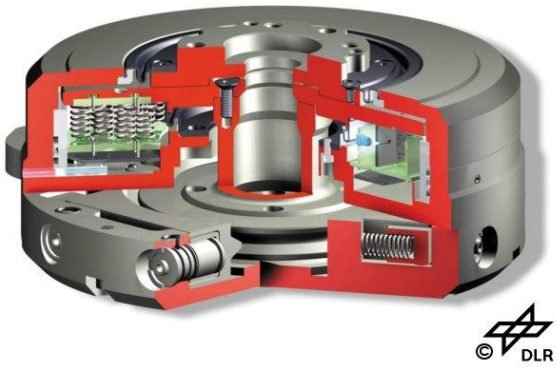

Figure 2.1: Force/Torque sensor

2.2 Impedance control

The impedance control is the most used control in physical human-robot interaction, this control has the purpose to makes the robot behaves has a generalized mass, spring, and dumper system. A big advantage of this control strategy is that allows to control the motion and the contact force at the same time.

Fist we have to define the mechanical impedance, that is the dynamical relationship between force and velocity (or displacement) for a mechanical system. In our case the impedance is the ration between the contact force resulted from interaction and the velocity of the manipulator, and in frequency domain the impedance $Z(s)$ can be written as [3]:

$$Z(s) = F(s)/\dot{X}(s) \tag{2.1}$$

Where $F(s)$ and $\dot{X}(s)$ are the Laplace transformation of the interaction force, and the manipulator velocity respectively. Substituting $\dot{X}$ with sX and rewriting equation (2.1), we obtain:

$$sZ(s) = F(s)/X(s) \tag{2.2}$$

And isolating $F(s)$:

$$F(s) = sZ(s) \cdot X(s) \tag{2.3}$$

From equation (2.3) is possible to notice that $F(s)$ and $X(s)$ cannot be controlled separately since they are related by $sZ(s)$, so the control strategy is based on the control $X(s)$ and the choice of the desired impedance behaviour through the tuning of Z(s). Normally, $Z(s)$ take the shape of:

$$Z(s) = Ms + D + K/s \tag{2.4}$$

Where M, D, K represent the inertia, dumping and stiffness value of the desired impedance behaviour; this impedance behaviour in time domain can be seen as:

$$M_d(\ddot{x}(t) - \ddot{x}_d(t)) + D_d(\dot{x}(t) - \dot{x}_d(t)) + K_d(x(t) - x_d(t)) = F(t) \tag{2.5}$$

Where M_d,D_d, K_d are the desired value of inertia, dumping and stiffness; $F(t)$ is the contact force; $x(t)$ is the actual position of the robot end effector and $x_d(t)$ is the desired position of the end effector.

2.3 Robot dynamic model in interaction with the environment

The dynamic model of a manipulator in interaction with environment in vector form can be described as follow:

$$B(q)\ddot{q} + C(q,\dot{q})\dot{q} + F_v\dot{q} + f_s(q,\dot{q}) + g(q) = \tau - J^T(q)h \tag{2.6}$$

Where:

- $\boldsymbol{q} \in \mathbb{R}^n$, $\dot{\boldsymbol{q}} \in \mathbb{R}^n$, $\ddot{\boldsymbol{q}} \in \mathbb{R}^n$ are vectors that contain the robot joints positions, speeds, accelerations of the manipulator; and n is the number of degrees of freedom of the robot;
- $\boldsymbol{B}(\boldsymbol{q}) \in \mathbb{R}^{n\times n}$ is the Inertia matrix of the manipulator that is symmetric, positive-definite and depend on q;
- $\boldsymbol{C}(\boldsymbol{q}, \dot{\boldsymbol{q}}) \in \mathbb{R}^{n\times n}$ is a matrix that contains the centrifugal and Coriolis term. The matrix C is not unique, however normally its elements are chosen following the Christoffel symbols method in order to achieves important proprieties of the dynamic model [4]. This matrix depends on joints positions and speeds;
- $\boldsymbol{F_v} \in \mathbb{R}^{n\times n}$ is a diagonal matrix that contains the viscous friction coefficients of the joints, and $-F_v\dot{q}$ represents the viscous friction torques;
- $\boldsymbol{f_s}(\boldsymbol{q}, \dot{\boldsymbol{q}}) \in \mathbb{R}^n$ is the function that represents the static frictions at the joints, normally this term is simplified as $F_s sgn(\dot{q})$;
- $\boldsymbol{g}(\boldsymbol{q}) \in \mathbb{R}^n$ represents the moments generated by the gravity at the joints axes in the current configuration, it depends by the vector of joints positions q;
- $\boldsymbol{\tau} \in \mathbb{R}^n$ is a vector that contains the actuation forces/torques at each joint;
- $\boldsymbol{J^T}(\boldsymbol{q}) \in \mathbb{R}^{r\times n}$ is the Jacobian matrix, and r is the dimension of the velocity vector. This matrix maps joints velocities into the end-effector velocities, according to the relation:

$$v = \begin{bmatrix} \dot{p} \\ \omega \end{bmatrix} = J(q)\dot{q} \tag{2.7}$$

  Where v is the velocity vector; $\dot{p}$, and ω are the linear and angular velocities of the tool frame. The Jacobian is called geometric, if the angular speed is expressed in a minimal representation;

- $\boldsymbol{h} \in \mathbb{R}^r$ is a vector that contains the resultants of external forces f and moments μ applied by the end effector on the environment, with respect to the origin of the end-effector frame, in formulas:

$$h = \begin{bmatrix} f \\ \mu \end{bmatrix} \tag{2.8}$$

2.4 Impedance control applied to a manipulator

The dynamic model of a manipulator in interaction with the environment is described by (2.6), and we use an inverse dynamic control law [4]:

$$\tau = B(q)y + C(q, \dot{q})\dot{q} + g(q) \tag{2.9}$$

Now substituting this expression in (2.6) we obtain:

$$\ddot{q} = y - B^{-1}(q)J^T(q)h \tag{2.10}$$

Where y is the control variable. The equation (2.10) represent a nonlinear coupling term due to external forces. We assume for y the expression used in the inverse dynamic control in the operational space [4]:

$$y = J_A^{-1}(q)(\ddot{x}_d + K_D\dot{\tilde{x}} + K_P\tilde{x} - \dot{J}_A(q,\dot{q})\dot{q}) \tag{2.11}$$

Where $J_A(q)$ is the geometric Jacobian matrix, x_d is the desired position, K_D and K_P are tuneable parameters respectively, and $\tilde{x}$ is:

$$\tilde{x} = x_d - x \tag{2.12}$$

By substituting the expression (2.11) in (2.10) we obtain the dynamics equation in closed loop:

$$\ddot{\tilde{x}} + K_P\dot{\tilde{x}} + K_D\tilde{x} = B_A^{-1}(q)h_A \tag{2.13}$$

Where $B_A(q)$ is:

$$B_A(q) = J_A^{-T}B(q)J_A^{-1} \tag{2.14}$$

Matrix founded in (2.14) represents the inertia matrix in the operational space. The h_A term represents is a vector that contain the generalized forces performing work on $\dot{x}$, and is related to h by the following relation:

$$h_A = T_A^T(x)h \tag{2.15}$$

With $T_A$that is the following matrix:

$$T_A = \begin{bmatrix} I_{3\times3} & 0_{3\times3} \\ 0_{3\times3} & T(\phi) \end{bmatrix} \tag{2.16}$$

Where $T(\phi)$ represents the transformation matrix from $\dot{\phi}$ to ω, and ϕ is a vector that describe the orientation in a minimal representation.
In equation (2.13) we have obtained an impedance relation which can be tuned by choosing a proper K_P and K_D for the dumping and stiffness contribution respectively, but this system is only partial assignable and also coupled. In order to solve these problems we have to measure the interaction forces with a force sensor, and ones the force measurements are available, is possible to slightly modify equations (2.9) and (2.10) in order to obtain the following ones:

$$\tau = B(q)y + C(q,\dot{q})\dot{q} + g(q) + J^T(q)h \tag{2.17}$$

and

$$y = J_A^{-1}(q)M_d^{-1}(M_d\ddot{x}_d + D_d\dot{\tilde{x}} + K_d\tilde{x} - M_d\,\dot{J}_A(q,\dot{q})\dot{q} - h_a) \tag{2.18}$$

Where M_d,D_d,K_d are diagonal and positive definite matricies. The term $-J_A^{-1}(q)M_d^{-1}h_a$ was introduced in (2.18) in order to obtain a linear impedance with respect to h_A, otherwise the term $J^T(q)h$ in (2.17) compensates exactely the external forces and makes the manipulator infinitely stiff concerning the contact forces.
Now we can use these two new equations to repeat the same procedure as before, and after some calculation we obtain:

$$M_d\ddot{\tilde{x}} + D_d\dot{\tilde{x}} + K_d\tilde{x} = h_A \tag{2.19}$$

With M_d,D_d,K_d that can be tuned to select the wanted inertia, dumping, and stiffness parameters of the mechanical impedance; in order to obtain the wanted behaviour. We have obtained in (2.19) a complitely decoupled and assignable system.

However, this approach has several issues:

- It requires a perfect knowledge of the dynamic model of the manipulator and a complete cancellation of nonlinearities and coupling terms;
- This method assume that the joints torques are complitely accessible;
- The system become compliant to external disturbance, while normally the industrial robots be not.

To solve these problems, we use an admittance filter, which convert a force into desired displacement, relying on the position control already present on the manipulator. In Figure 2.2 is possible to see how impedance control with admittance filter is implemented.

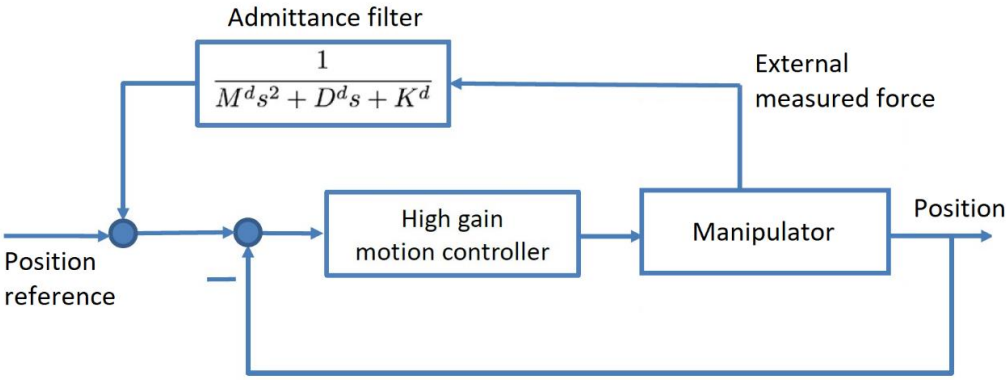

Figure 2.2: Impedance control with admittance filter.

Chapter 3

Human arm dynamic model

3.1 The reason of the dynamic model estimation

During a human- robot interaction normally an impedance control based on position control of the manipulator is used, however there is a condition for which the system formed by human and robot can become unstable. This unstable condition occours when the operation stiffs his arm, in this scenario the time delay of the movements of the robot or the operator makes the overall system unstable. To stabilize this condition the virtual impedance of the robot has to be retuned by increasing the stiffness or the dumping parameter of the impedance control. For this reason, normally viscosity or stiffness coefficent of the robot control are settled at high value, to prevent the system to fall into the previous mentioned unstable condition. Nevertheless, this solution is not an optimal one, since the choice of high impedance characteristic of the robot makes the collaboration more laborious, indeed the worker has to carry out the task with an extra load due to this parameters selection. To get an overall system that reduce the over load for the operator or that can solve some optimization problems, we need that the impedance control tune its parameters by looking at the stiffness of the operator's arm impedance at the wrist, so we can estimate the human arm impedance parameters and tune the impedance control parameters consequently to obtain the desired behaviour. This approach is called variable admittance control.

3.2 Reduced complexity impedance model of the human arm

In section 3.1 we have spoken about the advantages of estimating the human arm impedance parameters and also the importance to know the human arm stiffness, so in this section we will treat a computationally efficent cartesian stiffness model of human arm, based on the arm posture and the activation levels of biceps and triceps; i.e. the two dominant upper arm muscles.

First of all, we start by presenting the human arm impedance model:

$$M_H \ddot{x}_h + D_H \dot{x}_h + K_H x_h = F \tag{3.1}$$

Where $\ddot{x}_h, \dot{x}_h, x_h$are the acceleration, velocity, position of the human arm endpoint; and $M_H \in \mathbb{R}^{n_c \times n_c}$, $D_H \in \mathbb{R}^{n_c \times n_c}$, $K_H \in \mathbb{R}^{n_c \times n_c}$ are the inertia, dumping and stiffness term of the human arm respectively; and n_c is the dimension of the cartesian space; finally F is the interaction force. The inertia, dumping and stiffness matricies vary at the changing of the human arm configuration, muscle contraction level, etc; however the inertia term is

considered as constant [5], since we ignore the negligible effect of the muscle mass distribution in a neighbourhood of the predetermined arm configuration.

Now we want to explore the human arm endpoint stiffness parameter, which is the more interesting model part for a stability purpose.
In presence of constant muscular contraction, the arm geometry affects both the joint and the Cartesian stiffens behaviour. The joint stiffness is mainly due to changes in joint proprieties (as muscle and tendon length, moments arm, etc.), instead the Cartesian one needs an additional trasformation which requires the arm Jacobian. We explore a trasformation between two nearby equilibrium to investigate the arm geometry dependency of the two stiffness profiles [6] [7]:

$$\left[q_0, K_J(p, q_0), K_C(p, q_0)\right] \tag{3.2}$$

and

$$\left[q_0 + \delta q, K_J(p, q_0 + \delta q), K_C(p, q_0 + \delta q)\right] \tag{3.3}$$

The expression of the cartesian stiffness is:

$$K_C(p, q_0 + \delta q) = J^{+T}(q_0 + \delta q)\left[K_J(p, q_0 + \delta q) - G(q_0 + \delta q)\right]J^{+}(q_0 + \delta q) \tag{3.4}$$

Where $K_C \in \mathbb{R}^{6\times6}$ is the cartesian stiffness; $J \in \mathbb{R}^{6\times7}$ is the human arm Jacobian; $K_J \in \mathbb{R}^{7x7}$is the human arm joint stiffness; $q \in \mathbb{R}^7$ is the vector that contains the value of the joints angles; p is the co-contraction index which is considered constant in both the equilibria; q_0 is a vector that contains the initial value of the joints angles, therefore is the initial arm configuration; δq is the infinitesimal variation of joints angles between the two near equilibria. The last term $G(q)$ is defined as:

$$G(q) = \frac{\partial J^T(q) f_0}{\partial q} + \frac{\partial \tau_g(q)}{\partial q} \tag{3.5}$$

Where f_0 is the external load and $\tau_g(q)$ is the gravitational load. A rough estimation of gravitational load is:

$$\tau_g(q) = \sum_{i=1}^{n_J} J_{com_i}^T(q)\, g m_i \tag{3.6}$$

Where J_{com_i} is the centers of mass Jacobian of the ith joint of the human arm; m_i is the mass of the ith joint; g is the vector of gravitational acceleration; and n_J is the number of joints.

Now a Taylor expansion of the first order is applied to the cartesian stiffness expression (3.4):

$$K_C(p, q_0 + \delta q) = K_C(p, q_0) + \left.\frac{\partial K_C(p, q)}{\partial q}\right|_{q=q0} \delta q \tag{3.7}$$

And by computing the last term of the above equation we obtain:

$$\left.\frac{\partial K_C(p,q)}{\partial q}\right|_{q=q0} \delta q =$$
$$\left.\frac{\partial J^{+T}(q)}{\partial q}\right|_{q0} \delta q\left[K_J(p,q_0) - G(q_0)\right]J^{+}(q_0)$$
$$+ J^{+T}(q_0)\left[\left.\frac{\partial K_J(p,q)}{\partial q}\right|_{q0} \delta q\right. \tag{3.8}$$
$$\left. + \left.\frac{\partial G(q_0)}{\partial q}\right|_{q0} \delta q\right] J^{+}(q_0)$$
$$+ J^{+T}(q_0)\left[K_J(p,q_0) - G(q_0)\right]\left.\frac{\partial J^{+}(q)}{\partial q}\right|_{q0} \delta q$$

Is possible to notice, from the previous equation, that the pose-varying component of the joint stiffness matrix in cartesian coordinates is given by the only term:

$$J^{+T}(q_0)\left[\left.\frac{\partial K_J(p,q)}{\partial q}\right|_{q0} \delta q\right] J^{+}(q_0) \tag{3.9}$$

Watching at this term is possible to notice that the human arm Jacobian has a quadratic effect in Cartesian stiffness matrix behaviour; however far from the arm joints limits, in proximity of the middle ranges of the joints, the muscle length and the moment arm variations are small and bounded [6] [7]. Therefore, in a limited part of the human arm workspace the effect of the arm geometry in directional variations of the principal axes of the Cartesian stiffness ellipsoid is more effective than the configuration-dependent joint stiffness term, this implies that in the used model we consider the effect of the human arm Jacobian in directional variation of the arm endpoint stiffness ellipsoid on the major axes, while neglecting the contribution of the configuration-dependent joint stiffness matrix. This choice is made consequently to a compromise between accuracy and model complexity. As presented in [5] [8] [9], the modification in volume of the endpoint stiffness ellipsoid present a solid evidence of a contribution given by the coordinated stiffening of the arm joints, so to model the active joint stiffness regulation we use the term

$$K_J = c(p)\overline{K_J} \tag{3.10}$$

Where $c(p)$ is a size-adjusting co-contraction index and $\overline{K_J}$ is a constant matrix which correspond to the joint stiffness matrix at the minimum muscle activity, which can be experimentally achieved. For better visualization and understanding the $\overline{K_J}$ matrix can be divided into several 3 dimensional submatrices and subvectors [10]:

$$\overline{K_J} = \begin{bmatrix} K_{ss\,3\times3} & K_{es\,3\times2} & K_{ws\,3\times2} \\ K_{se\,2\times3} & K_{ee\,2\times2} & K_{we\,2\times2} \\ K_{sw\,2\times3} & K_{ew\,2\times2} & K_{ww\,2\times2} \end{bmatrix}_{7\times7} \tag{3.11}$$

Where the subscripts s,e,w stand for shoulder, elbow, and wrist respectively. The matrices on the main diagonal of the $\overline{K_J}$ matrix represent the single-joint stiffness, so the relative rotational joints stiffness of the shoulder, wrist, and elbow respectively. The other components of the $\overline{K_J}$ matrix represent the cross-joint stiffness, that is the cross-coupling effects between different physiological joints.

Finally, after all these considerations the model for the cartesian stiffness become:

$$K_C(p,q) = J^{+T}(q)\left[c(p)\overline{K_J} - G(q)\right]J^{+}(q) \tag{3.12}$$

We have obtained a computationally efficent method to compute online the human arm endpoint stiffness in 3D tracking the arm configuration and the co-contraction index.

3.3 Myo armbands

In the previous section we have founded computationally efficent method for the human arm impedance estimation in real-time. It needs the co-contraction index p, and the arm configuration q; both parameters can be founded by using two Myo armband. The Myo armband is a wearable gesture control device composed by 8 Medical Grade Stainless Steel EMG sensors, that can measure the muscles activities, and IMUs that contains accelerometer, gyroscope, magnetometer which are used to monitor arm movements. This armband has been developed by Thalmic Labs.

Figure 3.1: Myo armbands

In the human arm stiffness method, presented before, two Myo armbands are used: one positioned on the upper arm near the shoulder, and the other one at the half of the lower arm near the elbow. The armband on the upper arm is used to monitor the activity of the two dominant muscles of the arm (the triceps and biceps), using two of the eight EMG sensors; is also used to monitor the position of the upper arm using the integrated IMUs. The other armband is used only to monitor the motion and rotation of the lower arm. The position of both the parts of the arm are detected under the form of quaternions. We chose to use for the arm position detection the IMUs of two armband instead of a motion tracking based on vision sensors, because the second option may be significantly affected by occlusion during physical human robot interaction [11].

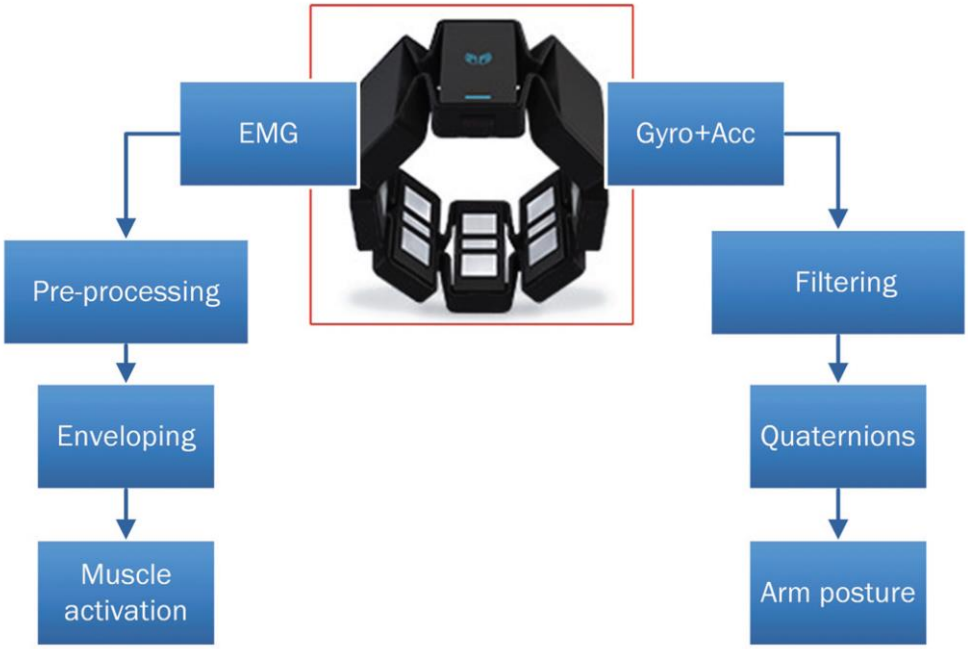

Figure 3.2: Signal collection from the Myo sensors

3.4 Human arm triangle

In this section we will describe how to pass from quaternions given by myo armbands to the human arm joints values using the human arm triangles model. First of all, we use a typical kinematic model defined using the Denavit and Hartenberg notation normally used for the manipulators. We use seven rotational joint to describe all the degree of freedom of the human arm: 3 DOF at the shoulder, 2 DOF at the elbow, 2 DOF at the wrist. In Figure 3.3 are represented the DH frame for each joint. In Table 3.1 are reported the DH parameters of this model, with the values between parentheses that indicate the offset of initial value of each joints angles.

$({}^{i-1}T_i)$	θ_i	d_i	α_i
0	-90°	0	-90°
1	θ_1(90°)	0	90°
2	θ_2(0°)	0	-90°
3	θ_3(90°)	l_u	90°
4	θ_4(0°)	0	-90°
5	θ_5(-90°)	l_l	90°
6	θ_6(90°)	0	-90°
7	θ_7(0°)	0	180°

Table 3.1: DH parameters of human arm kinematic model

For convenience the base frame is disposed with: the center of the frame in the center of the shoulder, the z_b axis in upward direction, the x_b axis in horizontal right direction, and the y_b axis is disposed in horizontal forward direction. The 7th frame has the center in the center of the palm, the z_7 axis overlaps at the normal vector to the palm plane, the x_7

axis points in direction of the fingers, and the y_7 axis complete the right-handed frame pointing in the opposite direction with respect to the thumb. Finally, l_u, l_l, l_h are the length of the upper arm, the length of the lower arm, and the distance from the center of the palm to the center of the wrist.

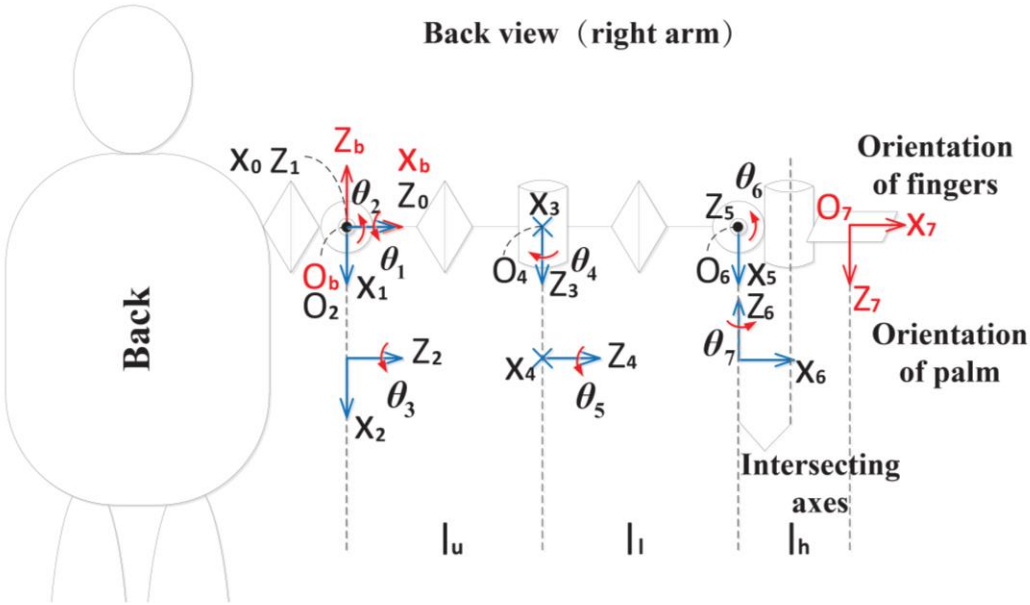

Figure 3.3: Human arm kinematic model

The seven joints of the DH model correspond to:

- **Joint 1**: shoulder inward/outward rotation;
- **Joint 2**: shoulder horizontal right lift/invers lift;
- **Joint 3**: shoulder outward/inward self rotation;
- **Joint 4**: elbow extension/flexion;
- **Joint 5**: elbow outward/inward self-rotation;
- **Joint 6**: wrist extension/flexion;
- **Joint 7**: wrist abduction/adduction

Completed the kinematic model of the arm is possible to define the human arm triangle model.

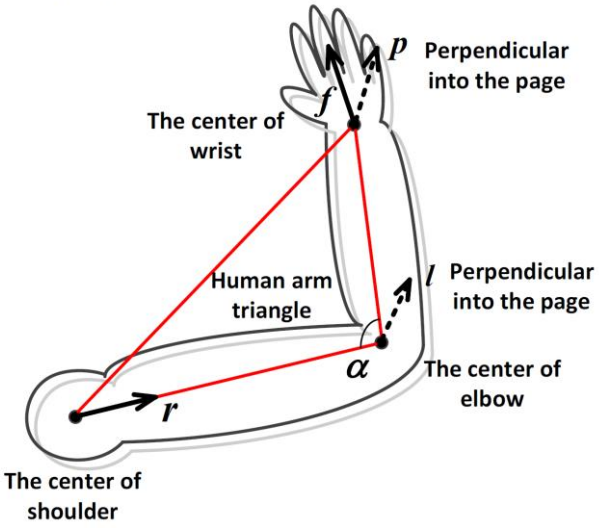

Figure 3.4: Human arm triangle

The human arm triangle can be expressed by five parameters (Figure 3.4):

- $\boldsymbol{r}$: is the unit direction vector of the upper arm;
- $\boldsymbol{l}$: is the unit normal vector of the plane of the human arm triangle determined by the right-hand screw in the direction of elbow extension.
- $\boldsymbol{\alpha}$: refers to the angle between the upper arm and lower arm;
- $\boldsymbol{f}$: is the unit vector in the direction of the fingers;
- $\boldsymbol{p}$: is the unit perpendicular to the palm plane, which point outward from the center of the palm.

It has been demonstrated in [11], [12] that the human arm triangle space spanned by these five parameters have a one to one mapping relationship with the seven degree of freedom kinematic model of the human arm presented before.

The method proposed in Section 3.2 with the Myo armband and their positioning on the human arm (Section 3.3), can only estimates the position of the upper arm and the lower arm, by finding l,r,α from the quaternions given by the IMUs present inside both armband. To do that we use a simplified version of human arm triangle model where the f and p parameters are not considered, so we can estimate the value of the three shoulder joints angles, and the two elbow joints angles. The last two joints angles, the ones of the wrist, are calculated by performing a simple inverse kinematic using the robot endpoint position and orientation, because the human arm is physically attached to the robot handle.

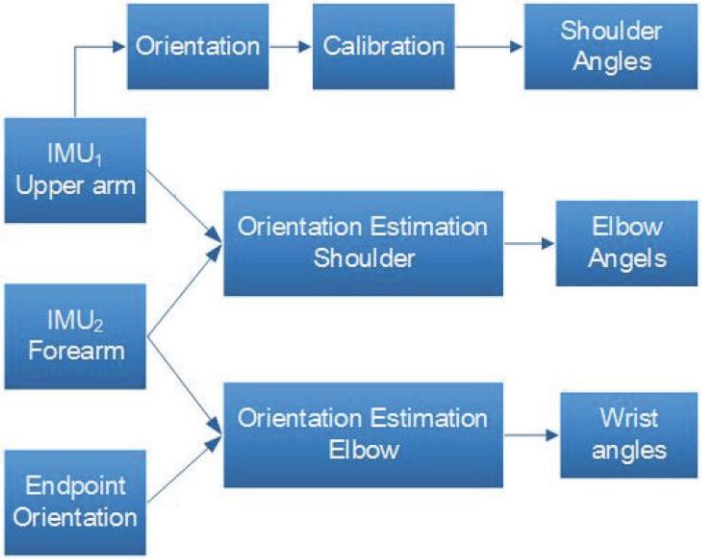

Figure 3.5: Joints angles estimation based on IMUs

3.4.1 Mappings from human arm triangle space to joint space

The locus of the center of the elbow is a spherical surface centered in the center of the shoulder, that is supposed to be known, with radius equal to the length of the upper arm and the motion of the elbow center is guaranteed by θ_1 and θ_2. However taking into account the range of motion of the upper arm joints, θ_1 stay between $0°\sim 360°$ and θ_2 between $-90°\sim 0°$, we just consider a hemispherical surface where the longitude is controlled by θ_1 and the latitude is controlled by θ_2, as is possible to see in the Figure 3.6.

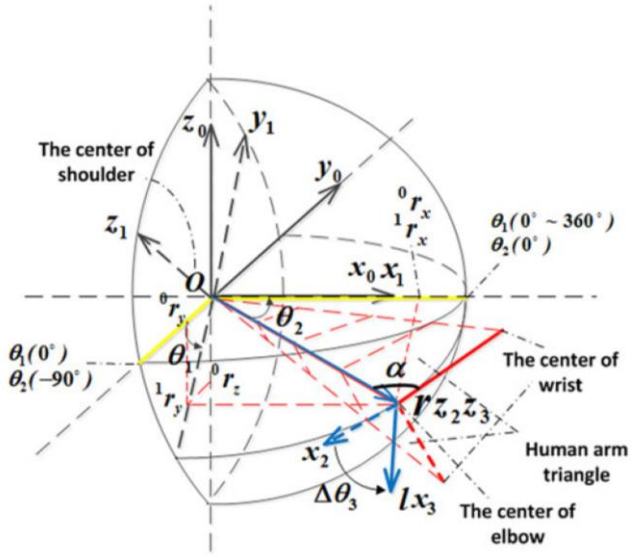

Figure 3.6: Algorithm representation of inverse mapping from human arm triangle sapce to joint space.

The algorithm starts from the frame $1\{Ox_1y_1z_1\}$, that is obtained by rotating frame $0\{Ox_0y_0z_0\}$ by θ_1 about the x_0 axis; and according to the right hand rule the positive rotational direction of θ_1 is in direction of x_0. In formulas:

$$\theta_1 = arccos\left(\frac{-{}^0r_y}{\sqrt{{}^0r_y^2 + {}^0r_z^2}}\right) \tag{3.13}$$

$$if: -{}^0r_z < 0, then: \theta_1 = 2\pi - \theta_1$$

Where ${}^0r = [{}^0r_x, {}^0r_y, {}^0r_z]^T$is the coordinate of the unit vector r of the upper arm represented in frame 0.

Then, the frame $2\{Ox_2y_2z_2\}$ is obtained by rotating frame 1 about z_1 axis by θ_2, and the positive rotational direction of θ_2 is along z_1 according to the right-hand rule. Now we have to express the unit vector r in frame 1 in order to find θ_2, and we proceed as follow:

$${}^1r = R^T(x, \theta_1) \cdot {}^0r \tag{3.14}$$

$$\theta_2 = -arccos\left(\frac{{}^1r_x}{\sqrt{{}^1r_x^2 + {}^1r_y^2}}\right)$$

Where $R^T(x, \theta_1)$ correspond to a rotational matrix around x of an angle of θ_1.

Next, we take in account for θ_3 and θ_4 that control the direction of the human arm triangle plane, and the angle between upper arm and forearm respectively. The ranges of these two terms are: $-90°\sim270°$ for θ_3, and $-180°\sim0°$ for θ_4. The frame $3\{Ox_3y_3z_3\}$ is obtained by rotating frame 2 about the z_2 axis by $\Delta\theta_3$, where $\Delta\theta_3 = \theta_3 - 90°$, and according to the right hand rule the positive rotation direction of $\Delta\theta_3$ is in direction of z_2 axis. We have obtained that the x_3 axis coincides with the parameter l of the human arm tringle. We can notice that the direction of the unit normal vector of the plane of the arm triangle when $\theta_3 = 90°$ is x_2, which in this particular case correspond to the tangential direction of the longitude at elbow center, so θ_3 can be calculated with the transformation matrix between frame 2 and 3 as follow:

$${}^0R_2 = (x_2, y_2, z_2), \quad {}^0R_3 = (x_3, y_3, z_3) \tag{3.15}$$

Where ${}^0R_3$ and ${}^0R_2$ are the transformation matricies from frame 3 and 2 to frame 0 respectively, and the value between parentheses are column vectors that correspond to axes of frame two and three represented in frame 0; also:

$$z_2 = z_3 = {}^0r, \quad x_3 = {}^0l \tag{3.16}$$

$$x_2 = R(x, \theta_1) \cdot (-\sin(-\theta_2), -\cos(-\theta_2), 0)^T$$

$$y_2 = z_2 \times x_2, \quad y_3 = z_3 \times x_3$$

And

$${}^2R_3 = {}^0R_2^T \cdot {}^0R_3 = R(z, \Delta\theta_3) \tag{3.17}$$

Then

$$\begin{cases} x_2 \cdot x_3 = \cos(\Delta\theta_3) \\ y_2 \cdot x_3 = sin(\Delta\theta_3) \end{cases} \tag{3.18}$$

Finally, we obtain

$$\Delta\theta_3 = \arccos(x_2 \cdot x_3) \tag{3.19}$$

$$if: \ y_2 \cdot x_3 < 0, \qquad then: \ \Delta\theta_3 = -\Delta\theta_3$$

$$so\ \theta_3 = \pi/2 + \Delta\theta_3, \quad and \quad \theta_4 = \alpha - \pi$$

In conclusion we have obtained the values of the joints angles θ_1, θ_2, θ_3, θ_4, starting from the three parameters of the simplified human arm triangle model l,r,α.

This algorithm can be expanded in order to find the last three joints angles values by knowing the wrist center, that can be found by the reduced algorithm considered above, and the last two parameters of the human arm tringle f and p, but for the estimation method presented in this thesis this expansion is not used.

3.5 Procedure to identify constant model parameters

In this section we describe the procedure to identify the parameters which have to be identified offline and are needed for the reduced complexity model of the human arm. These parameters are: the minimum activation joint stiffness matrix $\overline{K_J}$, and the co-contraction index $c(p)$ both presented in section 3.2. To identify these two parameters, first we assume that $J(q)$, $G(q)$ are known and $f_0 = 0$, so there is no external load; then we follow the standard technique for the identification of human arm endpoint stiffness in 3D [13], that consist in applying stochastic perturbation to the human wrist through a handle while the restoring forces are recorded using a 6-axis force/torque sensor.

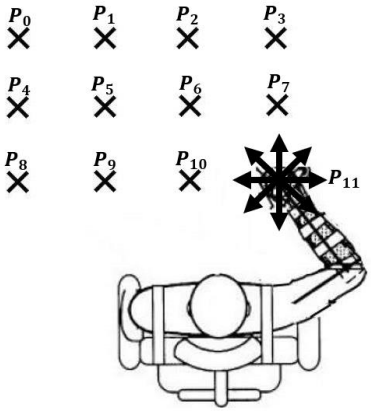

Figure 3.7: Example of test locations

This experiment is carried out in different arm configuration and in a reasonable arm workspace, avoiding joints limits and singular configurations, and at different co-contraction levels. These configurations are chosen anterior to the coronal plane of the

operator (an example can be seen in Figure 3.7). In each wrist center position the shoulder wrist configuration is allowed to vary within the redundant manifold, in order to realize measurment with different elbow height (an example of the arm redundant manifold can be seen in Figure 3.8). For each configuration of the arm the operator modulates and keeps the co-activation level of the arm muscles in different levels: low-activity, mid-activity, and high-activity. These levels are calculated as a predetermined percentage of the maximum one, and in order to keep the right co-activation value the operator is helped by a screen that display the EMG signals.

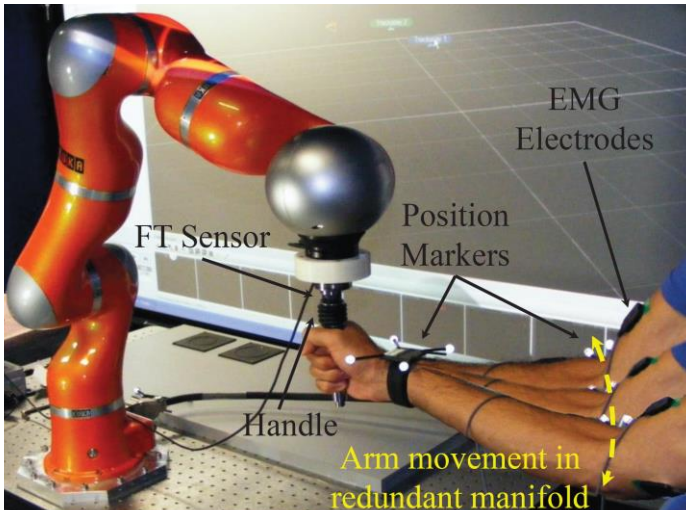

Figure 3.8: Example of redundant manifold of human arm in experimental setup

The muscle co-activation index p is obtained by a low pass filter and a moving average process applied to the extracted EMG signals coming from the two of eight channel closest to the two dominant muscle of the human arm (biceps and triceps). In order to describe the co-activation levels we use the following equation:

$$p(k) = \frac{1}{W_s}\left(\sum_{k=1}^{W_s-1} E_B(t-k) + \sum_{k=1}^{W_s-1} E_T(t-k)\right) \tag{3.20}$$

Where W_s is the window size, E_B and E_T are the amplitudes of the enveloped EMG signals of Biceps and Triceps respectively, t is the current sampling time, and k is the sample point.

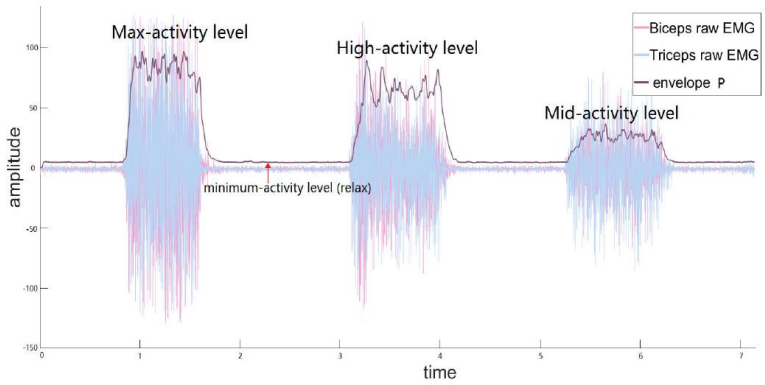

Figure 3.9: Example of the envelope of co-activation index p obtained by moving average process and low pass filter.

Before deriving the $\overline{K_J}$ and $c(p)$ parameters we have to focus on the dynamical relation between the arm endpoint displacements and the restoring forces, which can be described by the following relation:

$$F = \begin{bmatrix} F_x(f) \\ F_y(f) \\ F_z(f) \end{bmatrix} = \begin{bmatrix} G_{xx}(f) & G_{xy}(f) & G_{xz}(f) \\ G_{yx}(f) & G_{yy(f)} & G_{yz}(f) \\ G_{zx}(f) & G_{zy}(f) & G_{zz}(f) \end{bmatrix} \begin{bmatrix} x(f) \\ y(f) \\ z(f) \end{bmatrix} \tag{3.21}$$

Where F_x, F_y, F_z are Fourier transforms of the endpoint forces along the axes of the Cartesian reference frame; with x, y, z that are the Fourier transforms of the human arm endpoint displacements in the Cartesian directions. To identify each transfer functions G_{ij} we adopt a second order, parametric, linear model as below:

$$G_{ij} = I_{Hij}s^2 + D_{Hij}s + K_{Hij}, \quad s = 2\pi f\sqrt{-1} \tag{3.22}$$

Where the I_H, D_H, K_H are the human arm endpoint inertia, viscosity and stiffness matricies. The parameters of G_{ij} are identified using the least squares algorithm in frequency range $0{\sim}10\ Hz$ [14].

Consequently, all the stiffness matricies K_H obtained from tests that correspond to the minimum co-activation level are used to obtain the $\overline{K_J}$ matrix by minimizing the Frobenius norm below:

$$\left\|\overline{K_J} - J^T(q)K_H(p,q)J(q) - G(q)\right\| \tag{3.23}$$

Where, as we said before, the external load are supposed to be zero ($f_0 = 0$) and so $G(q) = \frac{\partial \tau_g(q)}{\partial q}$.

The other K_H, the ones obtained with mid and high muscular activation levels, are used to identify the constant parameters of $c(p)$, c_1 and c_2 by minimizing the Frobenius norm that follow:

$$\left\|c(p)\overline{K_J} - J^T(q)K_H(p,q)J(q) - G(q)\right\| \tag{3.24}$$

With $c(p)$ expressed as:

$$c(p) = 1 + \frac{c_1(e^{-c_2 p} - 1)}{(e^{-c_2 p} + 1)} \tag{3.25}$$

Finally, once obtained both $\overline{K_J}$ and $c(p)$ the online estimation of human arm endpoint stiffness matrix can be done using (3.12)

One last comment on this impedance estimation method is on the dumping term, since as reported in [15] from the experimental results, the change of dumping matrix is not obvious within a small range of the muscle activation level centered at each level (low, mid, high). Therefore, we assume that the continuous trajectory of the damping matrix can be discretize in three different matricies corresponding to three different muscle activation levels for each arm configuration; so is possible to build a look-up table among the dumping matrix, arm configuration, and the muscle activation level, in a certain range based on experimental data.

Chapter 4

Simulation

In this chapter we will speak about the simulation part, that mainly consist in the derivation of the constant parameters to fit the model of section 3.2 from data of Table 4.1 and then compare the stiffness estimation results, of the proposed method and a previously used one, on a human arm linear trajectory.

The data used for the parameters estimation of the proposed method are taken from [16], where the procedure used for the data acquisition is similar to the one proposed in section 3.5, but with two slightly differences. These differences are: the subject's arm is positioned in a planar posture with the elbow sustained, and the motion of the wrist is constrained to remain fixed with a wristband. The reasons of these differences are due to the fact that the previous stiffness estimation method work only in a planar condition. The data of Table 4.1 have been collected to be used with this method, consequently is possible to notice that the stiffness matricies founded from experiments are only two by two, since from this type of experiments only the planar stiffness can be found. The experiments are made in 4 different levels of co-activation levels of the human arm muscles, which are 0%, 25%, 50%, 75%; and in twelve different arm postures. However not all the experimental positions in Table 4.1 can be used for simulations, since P_0, P_4, P_{11} are characterized by strange behaviours; this may be because they are singular arm postures. These three positions with P_1, P_8, P_9 are not used in the simulations because they are considered not enough reliable.

Arm posture	0%	25%	50%	75%
0	$\begin{bmatrix} 606.5 & 1454.6 \\ 166 & 1592.5 \end{bmatrix}$	$\begin{bmatrix} 967.5 & 1861.7 \\ 188.1 & 2023.6 \end{bmatrix}$	$\begin{bmatrix} 1151.4 & 2040 \\ 232.5 & 2420.8 \end{bmatrix}$	$\begin{bmatrix} 1052.9 & 1840.4 \\ 180.7 & 2434.7 \end{bmatrix}$
1	$\begin{bmatrix} 589.7 & 998.2 \\ 196 & 1068.4 \end{bmatrix}$	$\begin{bmatrix} 921.8 & 1343.8 \\ 295.4 & 1463.7 \end{bmatrix}$	$\begin{bmatrix} 1191.9 & 1766.3 \\ 212.8 & 1853.1 \end{bmatrix}$	$\begin{bmatrix} 999.8 & 1956.9 \\ 74 & 2352.2 \end{bmatrix}$
2	$\begin{bmatrix} 838.3 & 1355.8 \\ 264.1 & 1192.8 \end{bmatrix}$	$\begin{bmatrix} 1102.9 & 1858.3 \\ 182.1 & 1623.6 \end{bmatrix}$	$\begin{bmatrix} 1538.8 & 2215 \\ 217.1 & 1996 \end{bmatrix}$	$\begin{bmatrix} 1776.8 & 2744.1 \\ 105.3 & 2652 \end{bmatrix}$
3	$\begin{bmatrix} 1277.5 & 1614.6 \\ 562.4 & 1192.8 \end{bmatrix}$	$\begin{bmatrix} 1102.9 & 1858.3 \\ 182.1 & 1623.6 \end{bmatrix}$	$\begin{bmatrix} 1538.8 & 2215 \\ 217.1 & 1996 \end{bmatrix}$	$\begin{bmatrix} 1776.8 & 2744.1 \\ 105.3 & 2652 \end{bmatrix}$
4	$\begin{bmatrix} 407.7 & 934.1 \\ 168.2 & 1274.2 \end{bmatrix}$	$\begin{bmatrix} 1681.5 & 2062.9 \\ 553.4 & 1468.2 \end{bmatrix}$	$\begin{bmatrix} 1950.4 & 2231.9 \\ 468 & 1567.3 \end{bmatrix}$	$\begin{bmatrix} 2337.7 & 2465.6 \\ 570.6 & 1989 \end{bmatrix}$
5	$\begin{bmatrix} 407.7 & 934.1 \\ 168.2 & 1274.2 \end{bmatrix}$	$\begin{bmatrix} 787.9 & 1348.6 \\ 178.5 & 1634.2 \end{bmatrix}$	$\begin{bmatrix} 1004.4 & 1508.4 \\ 215.3 & 1818.4 \end{bmatrix}$	$\begin{bmatrix} 801 & 1328.5 \\ -52.8 & 1813.5 \end{bmatrix}$
6	$\begin{bmatrix} 239.4 & 1337.5 \\ -158.1 & 1825.6 \end{bmatrix}$	$\begin{bmatrix} 626.5 & 1652.3 \\ -101.2 & 2131.7 \end{bmatrix}$	$\begin{bmatrix} 779.2 & 2134.9 \\ -44.2 & 2790.2 \end{bmatrix}$	$\begin{bmatrix} 938.2 & 2152.7 \\ -46 & 2957.1 \end{bmatrix}$
7	$\begin{bmatrix} 584.6 & 1119.6 \\ 166.5 & 1387.4 \end{bmatrix}$	$\begin{bmatrix} 1033.6 & 1631.8 \\ 360.1 & 1721.1 \end{bmatrix}$	$\begin{bmatrix} 1289.5 & 1763.1 \\ 321.5 & 1790.2 \end{bmatrix}$	$\begin{bmatrix} 1159.3 & 2273.2 \\ 377.7 & 2449.8 \end{bmatrix}$
8	$\begin{bmatrix} 825.3 & 1110.6 \\ 251.1 & 1073.3 \end{bmatrix}$	$\begin{bmatrix} 1040.2 & 1507.7 \\ 170.3 & 1724.3 \end{bmatrix}$	$\begin{bmatrix} 1190 & 1655.7 \\ 200.1 & 1940.6 \end{bmatrix}$	$\begin{bmatrix} 1217.5 & 1462.8 \\ -123.9 & 2384.1 \end{bmatrix}$
9	$\begin{bmatrix} -54.3 & 906.3 \\ -504.3 & 1626.8 \end{bmatrix}$	$\begin{bmatrix} 157.2 & 1230.3 \\ -608.7 & 2220 \end{bmatrix}$	$\begin{bmatrix} 324.9 & 1584.1 \\ -681.4 & 3065.6 \end{bmatrix}$	$\begin{bmatrix} 608.8 & 1984 \\ -876.7 & 3490.2 \end{bmatrix}$
10	$\begin{bmatrix} 425.3 & 1169.9 \\ -40 & 1815.3 \end{bmatrix}$	$\begin{bmatrix} 791.5 & 1572.6 \\ -84.9 & 2515.1 \end{bmatrix}$	$\begin{bmatrix} 824.8 & 1748.6 \\ -243.4 & 2905.1 \end{bmatrix}$	$\begin{bmatrix} 1045.6 & 2101.8 \\ -276.8 & 3403.5 \end{bmatrix}$
11	$\begin{bmatrix} 698.2 & 1303.6 \\ 82.1 & 1970.4 \end{bmatrix}$	$\begin{bmatrix} 1069.8 & 1603 \\ -116.7 & 2708.6 \end{bmatrix}$	$\begin{bmatrix} 1089.4 & 1558.7 \\ 113.7 & 2310 \end{bmatrix}$	$\begin{bmatrix} 1277 & 1849 \\ -19.3 & 2868.4 \end{bmatrix}$

Table 4.1: Endpoint stiffness estimation data.

4.1 Proposed stiffness estimation model simulation

In this section the explanation of all the code used to: simulate the arm, and find all the parameters by solving optimization problems. All the human arm structure simulations are done in MATLAB using the robotics toolbox [17] and the optimizations are done using the optimization toolbox [18].

4.1.1 Construction of the human arm model

The operator's arm has been modelled using the same procedure used for industrial manipulator; by using the DH parameters of Table 3.1, and the positions of the frames as in Figure 3.3; both presented in section 3.4. To simulate the kinematic model of the human arm the robotics toolbox [17] has been used. The initial position of the operator's arm is chosen to be:

$$q_{init} = \left[\frac{\pi}{2} \quad 0 \quad \frac{\pi}{2} \quad -\frac{\pi}{2} \quad -\frac{\pi}{2} \quad \frac{\pi}{2} \quad 0\right] \tag{4.1}$$

Where q_{init} represents the vector of joints angles. This choice is done to start with a configuration similar to the experimental one and to have a starting point for the kinematic inversion. To complete the model, as reported in Table 3.1, I need three parameters l_u, l_l, l_h that are: the length of the upper arm, the length of the lower arm, and the distance from the center of the palm to the center of the wrist. These parameters are not measured during the experiments because the previous method does not need to know the arm posture. However, the operator during the experiments was a woman, so to fill this gap I search in literature for a model that knowing the height of the subject gives the arm length parameters [19]. The height of the subject is also unknown and so I search for the mean height of woman in Italy and is about 163.5 [20]. Now the operator's arm can be represented, and the initial configuration can be seen in Figure 4.1.

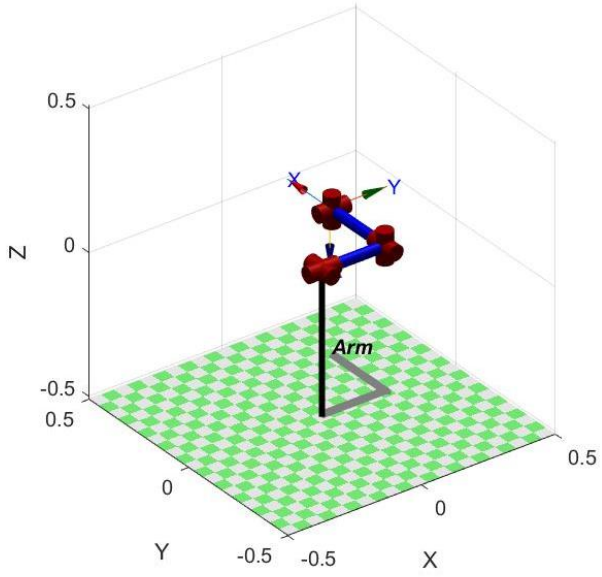

Figure 4.1: Initial configuration of operator's arm

Completed the kinematical part of the robot model I have focused on the dynamical part; since for the proposed parameter estimation of the stiffness model, the gravitational load of the human arm is requested. As for the arm lengths, the mass and the center of mass of the operator's arm have not been measured. As before, to find these parameters, I have searched in the literature for a relationship between the weight of the subject and the weights and center of mass positions of upper arm, lower arm, and hand; I have found these parameters relationship in [21]. To complete the dynamic model I have to choose a weight of the subject, to do that I have searched for the mean weight of the woman in Italy that is about 59 Kg, as is possible to see in [22]. For sake of semplicity I have considered the weight of the hand added inside the weight of the lower arm, with a slightly modification of the center of mass of the lower arm.

Obtained all these center of mass positions and the arm portions weights, the human arm dynamic model has added to the kinematic one obtaining the human arm model.

4.1.2 Inverse kinematic and gravitational load

The kinematic inversion is done in all the points where the experiment was carried out, so $P_2, P_3, P_5, P_6, P_7, P_{10}$. These points are identified starting from the base frame centered in the shoulder and each point is 10 cm away from the nearest ones and from the base frame as is possible to see in Figure 4.2.

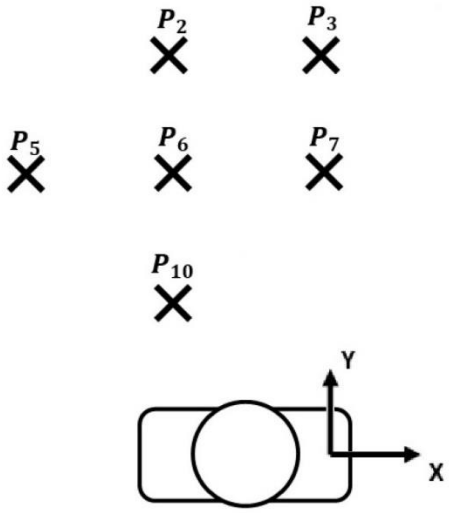

Figure 4.2: Trials point positions.

The kinematic inversion can be executed using the $ikcon()$ function of robotics toolbox [17], this function has been chosen since the arm is redundant and so the kinematic inversion can give infinite results, however this function makes the invers kinematic by optimization considering the joints limits. Therefore, imposing to the joint 2 to remain still at 0 and using as initial position q_{init}, we obtain that the shoulder remains right lifted for all the kinematic inversions, and so we obtain the same arm postures as in the experiments. Once the vector of joints angles is known, with the function $jacob0()$ the Jacobian was extracted. The results of the kinematic inversion are presented in Figure 4.3 below.

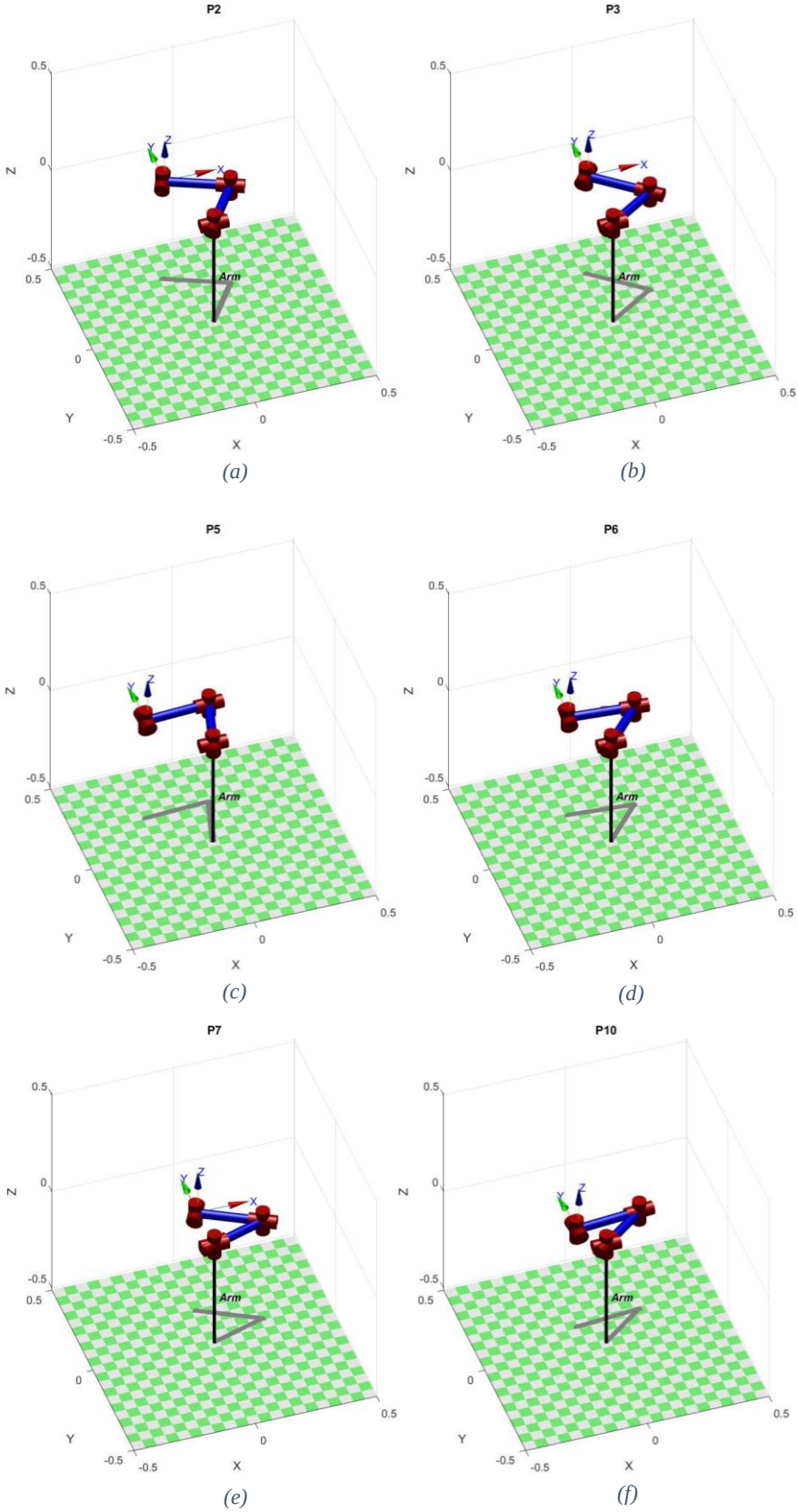

(a) *(b)* *(c)* *(d)* *(e)* *(f)*

Figure 4.3: Results of kinematic inversion of: P2 (a), P3 (b), P5 (c), P6 (d), P7 (e), P10 (f).

Once the kinematic inversions are completed, the gravitational load can be computed. For this term, no function of the robotics toolbox can help us to find the analytic expression of the gravitational load, to then differentiate it and obtain the $G(q)$. To fill this gap I use the symbolic math toolbox, which allow to manipulate and solve symbolic expression, to generate the symbolic expression of the gravitational load according to equation (3.6), and the center of mass Jacobians are calculated with the data used to build the dynamic model of the human arm in section 4.1.1. Once the $\tau_g(q)$ analytical expression has been computed I proceed to differentiate it with respect to the vector of the joints angles q; in this way the analytical expression of the $G(q)$ term has been computed and by substituting the values of q founded by the kinematic inversion I obtain the values of $G(q)$ in all the trials points of the experiments.

4.1.3 Calculation of constant parameters

The calculation of the constant parameters has been done according to the equations (3.23) and (3.24), by imposing the relative optimization problems.

The first parameter obtained using the optimization toolbox [18] was $\overline{K_J}$, that is the constant joint stiffness matrix at minimum co-contraction. Firstly, I create a symbolic decision variable with the shape of a seven by seven matrix, which represent $\overline{K_J}$ that has to be minimized. As reported in section 3.5 the objective is to minimize the Frobenius norm below:

$$\left\|\overline{K_J} - J^T(q)K_H(p,q)J(q) - G(q)\right\|$$

To do that I use the following objective function:

$$\sum_i tr\left(\begin{matrix}\left(\overline{K_J} - J^T(q_i)K_i(p(0\%),q_i)J(q_i) - G(q_i)\right)^T \cdot \\ \cdot\left(\overline{K_J} - J^T(q_i)K_i(p(0\%),q_i)J(q_i) - G(q_i)\right)\end{matrix}\right) \tag{4.2}$$

Where $i = 2,3,5,6,7,10$ and correspond to the considered trials points of experiments, $p(0\%)$ is the value of co-activation index at the minimum value, and tr stands for the trace of the matrix. This function has to be minimized in $\overline{K_J}$.

For this optimization problem only inequality constraints have been used and are:

$$\overline{K_J}(1,1), \overline{K_J}(2,2), \overline{K_J}(3,3), \overline{K_J}(4,4), \overline{K_J}(5,5), \overline{K_J}(6,6), \overline{K_J}(7,7) \geq 0 \tag{4.3}$$

These constraints mean that the main diagonal of the joint stiffness matrix at minimum level of co-contraction are all greater or equal to zero; this choice is done consequently to the composition that the matrix $\overline{K_J}$ have to assume [23].

In conclusion the overall optimization problem, to obtain the $\overline{K_J}$ matrix, become:

$$\begin{aligned}&\text{mininize}_{\overline{K_J}} \sum_i tr\left(\begin{matrix}\left(\overline{K_J} - J^T(q_i)K_i(p(0\%),q_i)J(q_i) - G(q_i)\right)^T \cdot \\ \cdot\left(\overline{K_J} - J^T(q_i)K_i(p(0\%),q_i)J(q_i) - G(q_i)\right)\end{matrix}\right), i = 2,3,5,6,7,10 \\ &subject\ to \qquad \overline{K_J}(j,j) \geq 0,\ \ j = 1,\dots,7\end{aligned} \tag{4.4}$$

The obtained $\overline{K_J}$ is:

$$\overline{K_J} = \begin{bmatrix} 0.0005 & 2.4119 & 0.0002 & 1.4311 & 0.0000 & 0.0000 & 0.0003 \\ 2.4056 & 86.7394 & -0.0092 & -119.7925 & 0.0001 & -0.0002 & -3.9878 \\ 0.0002 & -0.0033 & 0.0003 & 0.7116 & 0.0000 & 0.0000 & 0.0003 \\ 1.4331 & -66.8155 & 0.7139 & 117.7467 & -0.0001 & 0.0003 & 4.1865 \\ 0.0000 & 0.0000 & 0.0000 & 0.0000 & 0.0002 & 0.0000 & 0.0000 \\ 0.0000 & 0.0000 & 0.0000 & 0.0001 & 0.0000 & 0.0002 & 0.0000 \\ 0.0003 & -1.4735 & 0.0003 & 3.1206 & 0.0000 & 0.0000 & 0.1188 \end{bmatrix} \quad (4.5)$$

The stiffness estimation results with the other co-activation levels, 25%, 50%, and 75%, are used to identify the constant parameters $c1$ and $c2$ of the size-adjusting co-contraction index $c(p)$; as reported in equation (3.25). However, the EMG signals of the experiments are not available, because the EMG signals are directly transformed in a co-contraction index COC different from the index p used in the presented method. Below the COC expression is reported:

$$COC_{index} = \frac{EMG_{min}}{EMG_{max}} \cdot \frac{EMG_{min} + EMG_{max}}{2} \cdot 100 \quad (4.6)$$

Where EMG_{min} and EMG_{max} represents the minor and the major magnitude between the EMG signals coming from the biceps and triceps, these values can vary during the experiment.

To fill the above mentioned gap, I have built an optimization problem in order to substitute the not calculable index p with the available index COC in the equation (3.25). First, I have computed the value of the $c(p)$ index at 25%, 50%, and 75% making three different optimization problems. The first problem has as symbolic decision variables $c(p(25\%))$, the second one has $c(p(50\%))$, and the last one has $c(p(75\%))$. The goal of these problems is to minimize the Frobenius norm below:

$$\left\| c(p)\overline{K_J} - J^T(q)K_H(p,q)J(q) - G(q) \right\| \quad (4.7)$$

Using as $c(p)$ the symbolic variable corresponding to the co-contraction level considered, and $\overline{K_J}$ is the one founded by the previous optimization problem. The following objective function has to be implemented to minimize the above Frobenius norm:

$$\sum_i tr\left(\begin{pmatrix} \left(c(p(m))\overline{K_J} - J^T(q_i)K_i(p(m),q_i)J(q_i) - G(q_i) \right)^T \cdot \\ \cdot \left(c(p(m))\overline{K_J} - J^T(q_i)K_i(p(m),q_i)J(q_i) - G(q_i) \right) \end{pmatrix} \right) \quad (4.8)$$

Where $i = 2,3,5,6,7,10$, as before, represent the considered trials points of the experiment, while m is the level of muscular co-contraction and span between 25%, 50%, and 75%, and tr stands for the trace of the matrix. This objective function has to be minimized in c(p). Then, I impose the following inequality and equality constraints:

$$K_i(p(m),q_i) = J^{+T}(q_i)\left(c\big(p(m)\big)\overline{K_J} - G(q_i) \right) J^+(q_i) \quad (4.9)$$

As in the objective function $i = 2,3,5,6,7,10$ and $m = 25\%,\ 50\%,\ 75\%$. This constraints means that the value of $c(p)$ has to make this equation true and so we have to get about the same value of $K_i(p(m),q_i)$ as in the experiments. The inequality constraints are:

$$c\big(p(m)\big) \geq 1 \tag{4.10}$$

These constraints are due to the value assumed by the $c(p)$ index, since when the co-activation level is at the minimum this index is equal to 1, as I possible to see in [23].

So, the overall optimization problem, to obtain the value of $c(p)$ at different muscles co-activations level, is:

$$\begin{aligned} &\text{mininize}_{\overline{K_J}} \sum_i tr\left(\begin{pmatrix}\left(c(p(m))\overline{K_J} - J^T(q_i)K_i(p(m),q_i)J(q_i) - G(q_i)\right)^T \cdot \\ \cdot\left(c(p(m))\overline{K_J} - J^T(q_i)K_i(p(m),q_i)J(q_i) - G(q_i)\right)\end{pmatrix}\right), \\ &\qquad i = 2,3,5,6,7,10;\ \ m = 25\%, 50\%, 75\% \\ &subjected\ to \quad K_i(p(m),q_i) \\ &\qquad = J^{+T}(q_i)\left(c(p(m))\overline{K_J} - G(q_i)\right)J^{+}(q_i), \\ &\qquad i = 2,3,5,6,7,10;\ \ m = 25\%, 50\%, 75\%; \\ &\qquad c\big(p(m)\big) \geq 1, \quad m = 25\%, 50\%, 75\%\ ; \end{aligned} \tag{4.11}$$

The results of this optimization are:

$$\begin{aligned} c\big(p(25\%)\big) &= 1.1672; \\ c\big(p(50\%)\big) &= 1.3482; \\ c\big(p(75\%)\big) &= 1.5795; \end{aligned} \tag{4.12}$$

Once the $c(p)$ values at 25%, 50%, and 75% have been computed I proceed to formalize the last optimization problem that gives as result the values of the coefficients of c_1 and c_2.
The aim of this optimization problem is to minimize the following Frobenius norm:

$$\left\| c(p(m)) - 1 + \frac{c_1\left(e^{-c_2 COC(m)} - 1\right)}{\left(e^{-c_2 COC(m)} + 1\right)} \right\| \tag{4.13}$$

Where $COC(m)$ represents the value of the co-contraction index of the precedent method with m that span between 25%, 50%, and 75%, as before; the $c(p(m))$ takes values from the problem above. To minimize this norm, I have used the following objective function:

$$\sum_i tr\left(\begin{pmatrix}\left(c(p(m)) - 1 + \frac{c_1\left(e^{-c_2 COC(m)} - 1\right)}{\left(e^{-c_2 COC(m)} + 1\right)}\right)^T \cdot \\ \cdot\left(c(p(m)) - 1 + \frac{c_1\left(e^{-c_2 COC(m)} - 1\right)}{\left(e^{-c_2 COC(m)} + 1\right)}\right)\end{pmatrix}\right) \tag{4.14}$$

Where c_1 and c_2 are the symbolic variable of this problem. The values of the $COC(m)$ indexes at the four muscular co-activation level used in the experiment are taken from the graph in Figure 4.4, where the first peak is at 25%, the second one is at 50%, and the last one is at 75%, and the $COC(m)$ at the minimum co-activation level is obtained by the mean value of the graph values without considering the peaks.

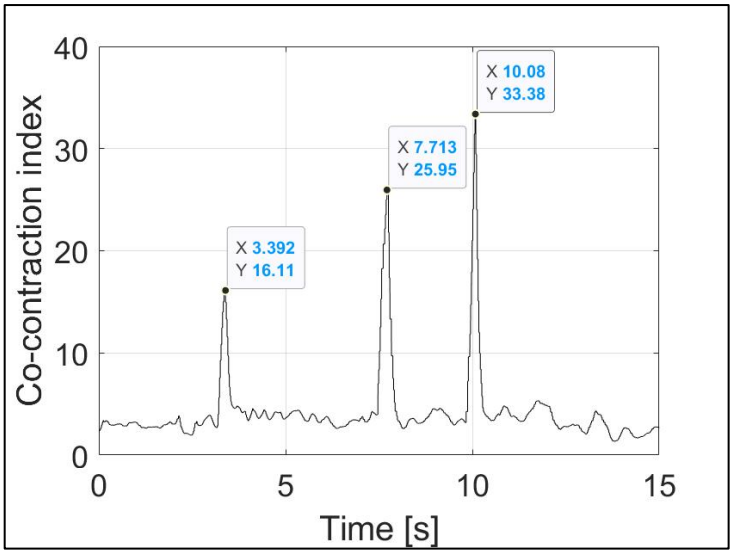

Figure 4.4: Levels of COC index at 0%, 25%, 50%, and 75%

The constraints for the problem are the following:

$$c\big(p(m)\big) = 1 + \frac{c_1\big(e^{-c_2 COC(m)} - 1\big)}{\big(e^{-c_2 COC(m)} + 1\big)} \tag{4.15}$$

Where we have imposed that with the founded coefficients, c_1 and c_2, the $c\big(p(m)\big)$ term is about the same that the one founded in the previous optimization problem at the same co-activation level. Also, I have imposed that:

$$c_1, c_2 \geq 0 \tag{4.16}$$

These conditions are imposed for the vale that these two parameters have to assume, as it possible to see in [24].

The overall control problem can be summarized as follow:

$$\begin{aligned} &\text{mininize}_{\overline{K_J}} \sum_i tr\left(\left(c\big(p(m)\big) - 1 + \frac{c_1\big(e^{-c_2 COC(m)} - 1\big)}{\big(e^{-c_2 COC(m)} + 1\big)}\right)^T \cdot \right. \\ &\left. \cdot \left(c\big(p(m)\big) - 1 + \frac{c_1\big(e^{-c_2 COC(m)} - 1\big)}{\big(e^{-c_2 COC(m)} + 1\big)}\right)\right), \\ &\qquad m = 25\%, 50\%, 75\%; \\ &subject\ to \quad c\big(p(m)\big) = 1 + \frac{c_1\big(e^{-c_2 COC(m)} - 1\big)}{\big(e^{-c_2 COC(m)} + 1\big)}, \quad m \\ &\qquad = 25\%, 50\%, 75\%; \\ &\qquad c_i \geq 0, \quad i = 1,2; \end{aligned} \tag{4.17}$$

The result of this optimization is:

$$c_1 = 2.0851e + 03 \tag{4.18}$$

$$c_2 = 1.4496e-05$$

Computed all these optimization problems we have all the term needed to estimate the human arm stiffness at the endpoint, by substituting in the equation (3.12) the parameters (4.5) and (4.18) obtained from the optimization problems above.

4.2 A brief comparison between two stiffness estimation methods

In this last section we will treat a comparison between the stiffness estimation method explained in this thesis with a previously used one [16].

4.2.1 The previous method

The previous stiffness estimation method simplifies the stiffness analysis by assume that there are no interferences between the two axes, so the terms outside the main diagonal of the stiffness matrix have been neglected. The terms on the main diagonal are obtained by the composition of two terms, the first one depends on the point of application and have the shape of a second order curve:

$$\begin{aligned} K_{hxx}(x_h,t)_{posture} &= p_{00_{xx}} + p_{10_{xx}}x_h + p_{01_{xx}}y_h + p_{20_{xx}}x_h^2 + p_{11_{xx}}x_h y_h \\ &\quad + p_{02_{xx}}y_h^2 \\ K_{hyy}(x_h,t)_{posture} &= p_{00_{yy}} + p_{10_{yy}}x_h + p_{01_{yy}}y_h + p_{20_{yy}}x_h^2 + p_{11_{yy}}x_h y_h \\ &\quad + p_{02_{yy}}y_h^2 \end{aligned} \tag{4.19}$$

the other term depends on co-contraction index:

$$\begin{aligned} K_{hxx}(x_h)_{COC} &= m_x \cdot COC_{index} \\ K_{hyy}(x_h)_{COC} &= m_y \cdot COC_{index} \end{aligned} \tag{4.20}$$

Where x_h is the human arm working point; $p_{ij_{xx}}$, $p_{ij_{yy}}$ are suitable coefficients; m_x, m_y are the linear coefficent of the x and y axes respectively; COC_{index} is the co-contraction index. Putting both togheter we obtain:

$$\begin{aligned} K_{hxx}(x_h,t) &= p_{00_{xx}} + p_{10_{xx}}x_h + p_{01_{xx}}y_h + p_{20_{xx}}x_h^2 + p_{11_{xx}}x_h y_h \\ &\quad + p_{02_{xx}}y_h^2 + m_x \cdot COC_{index} \\ K_{hyy}(x_h,t) &= p_{00_{yy}} + p_{10_{yy}}x_h + p_{01_{yy}}y_h + p_{20_{yy}}x_h^2 \\ &\quad + p_{11_{yy}}x_h y_h + p_{02_{yy}}y_h^2 + m_y \cdot COC_{index} \end{aligned} \tag{4.21}$$

The coefficients of this method are reported in the table below:

$p_{00_{xx}}$	$5.381e3$	$p_{00_{yy}}$	$4.497e3$
$p_{10_{xx}}$	$1.186e4$	$p_{10_{yy}}$	$1.357e4$
$p_{01_{xx}}$	$-1.06e4$	$p_{01_{yy}}$	$-1.011e4$
$p_{20_{xx}}$	$5.195e3$	$p_{20_{yy}}$	$1.226e4$
$p_{11_{xx}}$	$-2.164e4$	$p_{11_{yy}}$	$-2.38e4$
$p_{02_{xx}}$	$-5.539e3$	$p_{02_{yy}}$	$6.562e3$
m_x	10.2912	m_y	19.809

Table 4.2: Coefficients of previous method.

This coefficients of Table 4.2 are taken from the data in Table 4.1, so the same data are used to determine the parameters of both the methods and a comparison can be done.

4.2.2 The comparison

The comparison, between the two stiffness estimation method, has been done by simulating a linear path followed by the human arm with constant speed. The linear path, that can be seen in Figure 4.5, is from $P5$ to $P7$ and is done in $0.5[s]$ with a sampling time of $0.01[s]$.

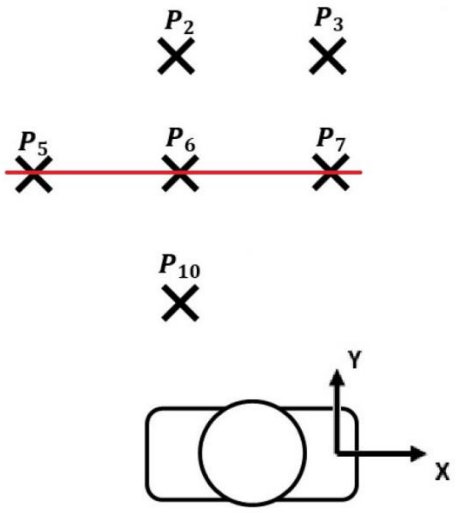

Figure 4.5: Simulated path

During the trajectory simulation the co-contraction level of the human arm muscles has been increased at $0.2\ [s]$ and it has been reset to the initial value at $0.3\ [s]$. In the following two graphs (Figure 4.6, and Figure 4.7) is possible to see the stiffness profile obtained with the two methods.

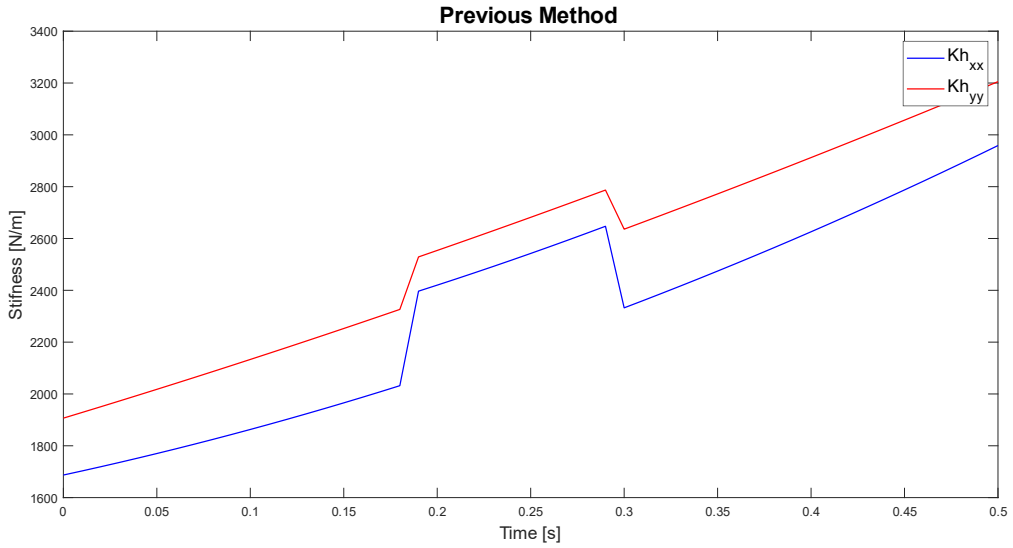

Figure 4.6: Stiffness simulation profile of the previous method.

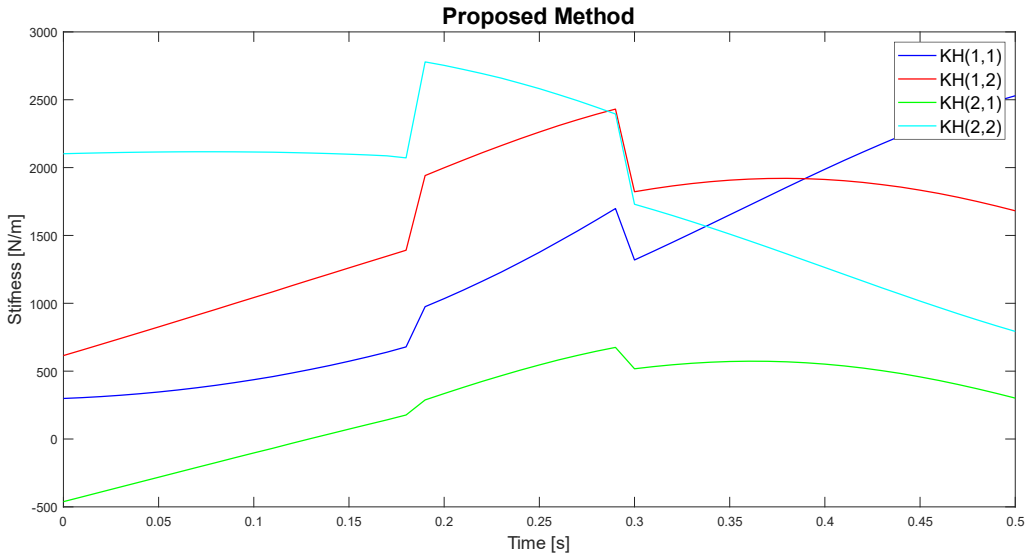

Figure 4.7:Stiffness simulation profile of the proposed method

From these two graph is possible to see that both the methods have the same behaviour when a change in co-contraction occours, indeed in both the graphs can be seen that the stiffness level increases when the co-activation level increases and when it decreases the stiffness is reduced accordingly. This behaviour is due to the coefficients that rescale the stiffness according to the co-contraction level, this two are: $K_{hii}(x_h)_{COC}$ for the previous method, and $c(p)\overline{K_J}$ in the proposed one.

The second difference of the two methods is the presence of the diagonal terms in the proposed one which are not considered in the previous one, this guaranteed lees neglected terms and so more precision and a better description of the stiffness.

The last consideration that can be done is on the diagonal terms of both the methods, in the previous method both the diagonal terms always increase, indeed in the proposed

one these two terms have more complex shapes. This means that the previous method is more conservative considering an always increasing stiffness profile, however the proposed stiffness description is more complex and describe more in depth the human arm endpoint stiffness without making the model more complex or laborious, and maintaining the ease of use.

Conclusions

In this thesis a human arm impedance mapping strategy was developed. This strategy is of particular interest in the field of human robot interaction, in combination with an adaptive impedance control, to make robot able to understand the human intention and act accordingly. In particular, the controller can be tuned in relation to the human arm impedance to avoid extra load for the operator during the cooperation, and to achieve some goals to improve the collaboration.
To accomplish that in this project, firstly, a human arm reduced complexity impedance model, based on the EMG parameters of the principal muscles of the operator's arm and on its configuration, was described with an explanation of the reasons of all the simplification introduced. Then, the tools for the acquisition of the data from the human arm, which are minimally invasive and easy to wear, were presented. At the same time, a kinematic and dynamic model for the human arm, similar to the one used for robotic manipulators, and a method to derive the human arm posture and its joints angles, in a simple and easily understandable way, were described. Later, the experimental procedures, to obtain the data to calibrate and identify the model parameters, was presented. These experiments are based on the perturbation method for the arm endpoint impedance estimation and have to be carried out in different arm configuration, and co-activation levels of the arm muscles. Next, all the procedures to obtain the human arm impedance model parameters from experiments were described, and they were later simulated using experimental data to verify the applicability of these procedures; the obtained impedance profile was compared with a previously used method, to underline the potentiality of the proposed one.

Further development

In this thesis a good starting point for the derivation of a reasonably simple and computationally efficent model for the human arm impedance was described; it can be improved by the:

- Use of more experimental data collected according to the procedure described in this thesis to validate the model;
- Use the proposed approach to tune the parameters of a variable impedance control;
- Use of more subject to verify the validity of the proposed method;
- Enlarge the impedance model workspace of validity by enhancing the model of the joint stifness matrix.

Bibliography

[1] International Organization for Standardization, “ISO 10218-1 (2011): Robots and robotic devices — Safety requirements for industrial robots — Part 1: Robots,” Geneva, Switzerland, July 2011.

[2] Markets and Markets, “Collaborative Robot (Cobot) Market by Payload, Component (End Effectors, Controllers), Application (Handling, Assembling & Disassembling, Dispensing, Processing), Industry (Electronics, Furniture & Equipment), and Geography – Global Forecast to 2026,” Mar 2020.

[3] P. Song, Y. Yu and X. Zhang, “Impedance Control of Robots: An Overview,” in *2nd International Conference on Cybernetics, Robotics and Control*, 2017.

[4] B. Sicigliano, L. Sciavicco, L. Villani and G. Oriolo, Robotics: Modelling, Planning and Control, Springer, 2009.

[5] A. Ajoudani, N. Tsagarakis and A. Bicchi, “Tele-impedance: Teleoperation with impedance regulation using a body–machine interface,” *The International Journal of Robotics Research,* 2012.

[6] A. Ajoudani, N. G. Tsagarakis and A. Bicchi, “On the role of robot configuration in cartesian stifness control,” *IEEE International Conference on Robotics and Automation,* June 2015.

[7] S.-F. Chen and I. Kao, “Conservative Congruence Transformation for Joint and Cartesian Stiffness Matrices of Robotic Hands and Fingers,” *Sage journals,* 2000.

[8] M. Turvey, “Action and perception at the level of synergies,” *Human Movement Scienze,* vol. 26, no. 4, pp. 657-697, 2007.

[9] M. Ison and P. Artemiadis, “Proportional Myoelectric Control of Robots: Muscle Synergy Development Drives Performance Enhancement, Retainment, and Generalization,” *IEEE Transactions on Robotics,* 2015.

[10] C. Fang, A. Ajoudani, A. Bicchi and N. G. Tsagarakis, “Online Model Based Estimation of Complete Joint Stiffness of Human Arm,” *IEEE Robotics and Automation Letters,* vol. 3, no. 1, 2018.

[11] C. Fang and X. Ding, “A Set of Basic Movement Primitives for Anthropomorphic Arms,” in *International Conference on Mechatronics and Automation*, Takamatsu, Japan, 2013.

[12] X. Ding and C. Fang, “A Novel Method of Motion Planning for an Anthropomorphic Arm Based on Movement Primitives,” in *IEEE/ASME Transactions on mechatronics,* 2013.

[13] E. J. Perreault, K. F. Robert and P. E. Crago, “Voluntary control of static endpoint stiffness during force regulation tasks,” *Journal of Neurophysiol,* vol. 87, pp. 2808-2816, 2002.

[14] A. Ajoudani, C. Fang, N. G. Tsagarakis and A. Bicchi, “A Reduced-Complexity Description of Arm Endpoint Stiffness with Applications to Teleimpedance Control,” in *IEEE/RSJ International Conference on Intelligent Robots and Systems (IROS)*, Hamburg, Germany, 2015.

[15] X. Chen, N. Wang, H. Cheng and C. Yang, “Neural Learning Enhanced Variable Admittance Control for Human-Robot Collaboration,” *IEEE Access,* vol. 8, pp. 25727-25737, 2020.

[16] M. Cavenaghi, Design of an adaptive admittance control for physical human-robot interaction in the lead-through programming collaborative task, 2017-2018.

[17] P. Corke, *Peter Corke. Robotics Toolbox for MATLAB Release 10.*, IEEE Robotics and Automation Magazine, 2017.

[18] J. Löfberg, *YALMIP toolbox for Matlab R20200930*, 2020.

[19] H. Dreyfuss, A. R. Tilley and S. B. Wilcox, The Measure of Man and Woman: Human Factors in Design, Whitney Library of Design, 1993.

[20] N. R. F. C. (NCD-RisC), “A century of trends in adult human height,” *eLife,* 2016.

[21] P. de Leva, “Adjustments to Zatsiorsky-Seluyanov's segment inertia parameters,” *Journal of Biomechanics,* vol. 29, no. 9, pp. 1223-1230, 1996.

[22] G. Pierlorenzi, L’ITALIA SI MISURA. UNA RISPOSTA DI POPOLO PER UN BENESSERE DIFFUSO, Aracne, 2015.

[23] C. Fang, A. Ajoudani, A. Bicchi and N. . G. Tsagarakis, “Online Model Based Estimation of Complete Joint Stiffness of Human Arm,” *IEEE ROBOTICS AND AUTOMATION LETTERS,* vol. 3, no. 1, pp. 84-91, 2018.

[24] X. Chen, C. Yang, C. Fang and Z. Li, “Impedance Matching Strategy for Physical Human Robot Interaction Control,” in *13th IEEE Conference on Automation Science and Engineering (CASE)*, Xi'an, China, 2017.

[25] International Federation of Robotics, “Demystifying collaborative industrial robots,” in *Positioning paper*, Frankfurt, Germany, 2018.

[26] A. Gasparetto and L. Scalera, “A Brief History of Industrial Robotics in the 20th Century,” *Advances in Historical Studies,* vol. 8, no. 1, 2019.

[27] WiredWorkers, [Online]. Available: https://wiredworkers.io/advantages-of-cobots/. [Accessed October 2020].

[28] S. Keeping, “Designing Collaborative Robots: Maximizing Productivity And Safety,” 27 August 2020.

[29] N. Pires, J. Ramming, S. Rauch and R. Araújo, “Force/Torque Sensing Applied to Industrial Robotic Deburring,” *ResearchGate,* 2002.

[30] A. Ajoudani, C. Fang, N. Tsagarakis and A. Bicchi, “Reduced-complexity representation of the human arm active endpoint stiffness for supervisory control of remote manipulation,” *The International Journal of Robotics Research,* vol. 37, pp. 155-167, 2018.